Impact of Ultrasonic Frequency on Aqueous Sonoluminescence and Sonochemistry

Michael A. Beckett and Inez Hua*

School of Civil Engineering, Purdue University, West Lafayette, Indiana 47907-1284

Received: September 13, 2000; In Final Form: December 8, 2000

A comprehensive investigation of ultrasonic frequency and its role in sonochemical activity and sonoluminescence (SL) has been performed. SL spectra and intensity were examined at four frequencies (205, 358, 618, and 1071 kHz) and in the presence of varying argon and oxygen saturation ratios. A series of high-energy reactions induced by the extreme temperatures and pressures obtained within a microbubble during acoustic cavitation contribute to the broad continuum characteristic of SL spectra. Chemical reactivity was also measured at all four frequencies. 1,4-Dioxane decomposition and hydrogen peroxide formation were chosen as representative sonochemical processes. A 358 kHz value was the optimal frequency for maximum SL intensity and chemical reaction rates. The impact of a hydroxyl radical scavenger, bicarbonate ion, on SL intensity and H_2O_2 formation was also examined. Results from this investigation indicate that nonlinear bubble implosions play a more significant role at lower frequencies whereas higher species flux rates influence chemical reactivity at higher frequencies.

Introduction

The ultrasonic irradiation of a solution induces acoustic cavitation, a transient process that promotes chemical activity. Acoustic cavitation is generated by the growth of preexisting nuclei during the alternating expansion and compression cycles of ultrasonic sound waves. In an aqueous liquid, temperatures as high as 4300 K and pressures over 1000 atm are estimated to exist within each gas and vapor-filled microbubble following an adiabatic collapse.[1,2] This phenomenon in turn initiates and promotes chemical reactivity through thermolysis, supercritical water oxidation, and free radical oxidation.[3] Thermolysis can take place within the bubble cavity and in the interfacial layer surrounding the cavity and is the central mechanism for generating free radicals.

An additional phenomenon, sonoluminescence (SL), is also induced during ultrasonic irradiation and has previously been used to probe the conditions within the bubble during and after rapid cavity expansion and implosion. Flint and Suslick[4] compared the observed spectra of SL from silicone oil with synthetic spectra modeled after known rotational and vibrational spectra of similarly excited diatomic emissions and found the effective cavitation temperature to be approximately 5000 K. Suslick et al.[2] have also investigated the SL spectra of metal carbonyls and have used this information to determine effective local pressures of approximately 1700 atm.[5]

A number of factors influence sonochemical activity and luminescence. These include frequency,[6−9] sparge gas,[10−12] ultrasonic power,[13−15] reactor pressure,[16] and solution temperature.[17−19] Individually, each of these factors may considerably affect the ultrasonic process and, when combined, may enhance ultrasonic effects.

Frequency is a significant factor in determining optimal reaction conditions. Currently, the influence of frequency on acoustic cavitation and sonochemistry is poorly understood. This article describes the results of a comprehensive assessment of frequency effects on sonochemical activity and SL performed under equivalent reactor conditions. The purpose of this investigation is to understand the impact of frequency and sparge gas on SL and sonochemical reactivity during ultrasonic irradiation. 1,4-Dioxane decomposition and hydrogen peroxide formation were chosen as representative sonochemical processes. 1,4-Dioxane is postulated to decompose in the interfacial region of a cavitation bubble,[20] and H_2O_2 formation is an indirect measure of •OH radical production during aqueous ultrasonic irradiation.[21] Finally, 1,4-dioxane is an organic pollutant, and its sonochemical degradation is of interest for environmental engineers. These chemical processes were used to elucidate the varying degree of cavitation reactivity at any given frequency. Frequency effects were further ascertained through the addition of bicarbonate ion, a hydroxyl radical scavenger, during sonication.

Experimental Section

Materials. Ultrapure water ($R = 18$ MΩ cm^{-1}) was obtained through a Barnstead NANOpure Ultrapure water system. Reagent grade potassium biphthalate (J.T. Baker, Inc.), potassium iodide (KI) (VWR Scientific), ammonium molybdate (Fisher Scientific), 1,4-dioxane (Sigma), ethylbenzene (Aldrich), and GC resolve grade hexane and methylene chloride (Fisher Scientific) were used as received. Fresh solutions of 1.0 mM 1,4-dioxane were used for each study. The experimental procedure for determining 1,4-dioxane decomposition rates is discussed elsewhere.[20]

Methods. A Cornerstone 130 monochromator (Oriel Instruments) equipped with a 1200-grooves/mm grating blazed at 250 nm and a resolution of 3 nm was used for medium-resolution studies of SL. The detector consisted of an Oriel Instruments side-on photomultiplier tube (PMT) powered by a 2000 VDC power supply and controlled by an OPM Multifunction Optical Power Meter (Oriel Instruments). TRAC32 Data Acquisition Software (Oriel Instruments) was used for spectral collection and analysis. All SL emission data was collected from 200 to 600 nm, and the intensities reported are from the average of

* To whom correspondence should be addressed. Phone: (765) 494-2409. Fax: (765) 496-1107. E-mail: hua@ecn.purdue.edu.

10.1021/jp003226x CCC: $20.00
Published on Web 03/27/2001

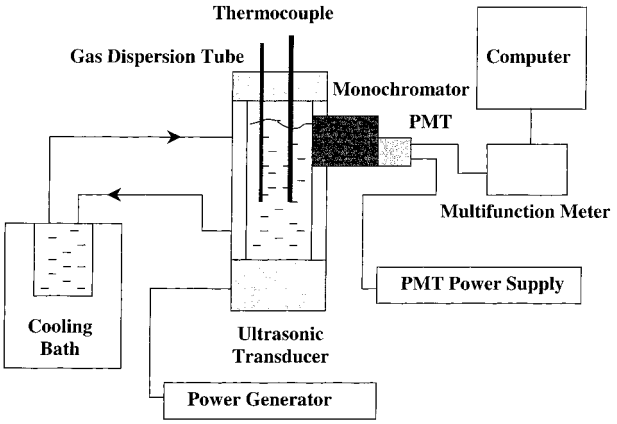

Figure 1. Schematic of experimental apparatus. The monochromator was fitted with a 1200-grooves/mm grating blazed at 250 nm. The side-on photomultiplier tube (PMT) was powered by a 2000 VDC power supply and controlled by an OPM Multifunction Optical Power Meter. The irradiated aqueous solutions were contained in a custom designed water-jacketed quartz reactor with an optical quartz interface connected to a circulating cooling bath for temperature control.

TABLE 1: Temperature Profiles during Sonication at Each Frequency (Temperature in $^{O}C \pm 0.5$ °C)

time (min)	205 kHz	358 kHz	618 kHz	1071 kHz
0	20	20	20	20
5	24.8	26.3	25.8	26.7
10	26.1	27.9	27.4	28.7
15	26.5	28.2	27.6	29.2
30	26.8	28.5	28.0	29.4
45	27.3	28.7	28.2	29.6
60	28.9	29.3	29.5	29.9

three spectral analyses. The monochromator was spectrally calibrated with a NIST-traceable standard mercury (Argon) lamp. The spectral response was calibrated using a QTH source (Oriel Instruments) in the range 200−600 nm. The monochromator was removed when determining emission intensity, thereby allowing for more sensitive detection measurements to be made with the PMT.

SL and sonolytic experiments were performed with an Allied-Signal URS 1000 ultrasonic transducer powered by an Allied Signal R/F generator LVG 60 (256 W maximum output). The instrumentation is shown in Figure 1. The effect of frequency on SL and chemical reactivity was investigated using the same transducer and reactor system for each experiment to maintain consistent power/area and power/volume ratios. Four ultrasonic frequencies were employed during the experiments (205, 358, 618, and 1071 kHz). The active acoustical vibration area of the transducer was 25 cm^2, and the output power of the generator (indicated on the instrument) was 128 W. Therefore, the effective transducer intensity during each experiment was 5.1 W/cm^2 (power/vibration area). The irradiated aqueous solutions were contained in a custom-designed water-jacketed quartz reactor with an optical quartz interface (Kontes Custom Glass) connected to a circulating cooling bath (Fisher Scientific). While the maximum volume for the reactor was 700 mL, the sonicated volume for each experiment was 500 mL.

Temperature profiles of the bulk liquid were taken to determine the equivalent amount of energy input at each frequency and are shown in Table 1. The energy delivered into the system was within 5% for all frequencies.

Sonochemical experiments involving H_2O_2 generation were performed in the batch mode by sonicating 500 mL of aqueous solution in the same quartz reactor used for SL measurements. The temperature was monitored continuously and maintained

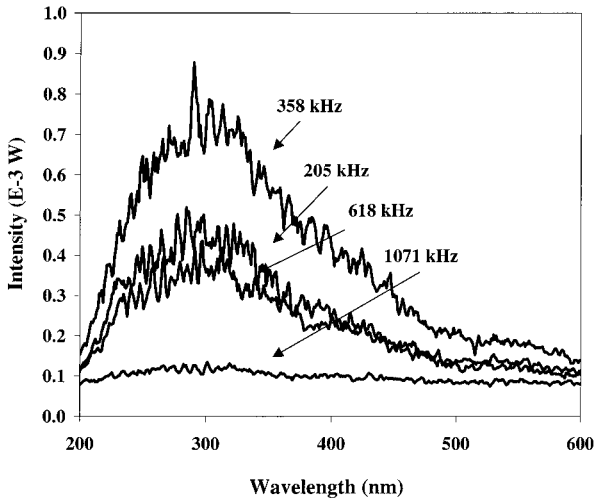

Reaction	Wavelength emission
1) $H_2O^* \rightarrow H_2O + h\nu_1$	380 –600 nm (λ_{max} ~ 425 nm).
2) $H_2O \rightarrow H^+ + {}^\bullet OH^* \rightarrow H^+ + {}^\bullet OH + h\nu_2$	λ ~ 280, 310, 340 nm λ ~ 200 – 400 nm
3) ${}^\bullet OH + M \rightarrow {}^\bullet OH^* + M \rightarrow {}^\bullet OH + h\nu_3$	λ_{max} ~ 310 nm
4) $H^+ + {}^\bullet OH + M \rightarrow [H \bullet\bullet\bullet OH \bullet\bullet\bullet M]^{\neq} \rightarrow H_2O + M + h\nu_4$	λ ~ 400 nm
5) $H_2O^* + 2\,M \rightarrow H_2O^{*}{}^\bullet M + M \rightarrow H_2O{}^\bullet M + M + h\nu_5$	λ < 300 nm.
6) $Ar + OH^* \rightarrow Ar{}^\bullet OH^*$ ($Ar{}^\bullet HO^*$) $\rightarrow Ar + OH + h\nu_6$	$Ar{}^\bullet OH^*$ (λ ~ 310, 316, and 318 nm) $Ar{}^\bullet HO^*$ (λ ~ 340 nm)

Figure 2. SL spectra at four discrete ultrasonic frequencies. Sparge gas = 100% Ar. Significant luminescence species are given by the reactions below the spectra.

at 25 °C. Four ports were located on the reactor cover and were used to fully saturate the solution with argon and/or oxygen, monitor liquid temperature, and withdraw samples periodically for analysis. Solutions were sparged 30 min prior to the beginning of each sonication at a gas flow rate of 100 mL/min and were continuously sparged throughout the entire run. The saturation gases included argon and oxygen and varied according to the type of experiment being performed.

Hydrogen peroxide was measured using the KI method of Kormann et al.[22] The iodide ion (I^-) reacts with H_2O_2 to form the triiodide ion (I_3^-) that absorbs strongly at 352 nm (ϵ = 26 000 M^{-1} cm^{-1}). The 2.0 mL sample aliquots from each experiment were mixed in a quartz cuvette containing 0.75 mL of 0.10 M potassium biphthalate and 0.75 mL of solution containing 0.4 M potassium iodide, 0.06 M sodium hydroxide, and 10^{-4} M anmonium molybdate. The mixed solutions (total volume = 3.75 mL) were allowed to stand for 2 min before the absorbance was measured. All absorbances were measured at 25 °C using a Perkin-Elmer Lambda 3 UV/vis spectrophotometer.

Results and Discussion

Aqueous Sonoluminescence. A series of spectra were obtained for the light emission of aqueous solutions under a variety of ultrasonic frequency and sparge gas conditions. SL spectra in the presence of 100% Ar are shown in the range 200−600 nm for all frequencies in this study (Figure 2). With the exception of 1071 kHz, the spectrum at each frequency exhibits the emergence of a broad continuum beginning at 200 nm and continuing through 500 nm while peaking at approximately 300 nm. A frequency of 358 kHz yields the broadest spectrum and greatest intensity at 300 nm, followed by 205 and 618 kHz. The spectrum for 1071 kHz appears diminished relative to the other three frequencies but exhibits similar features that are apparent when examined at a different scale. Spectra were also taken of luminescence in the presence of different mixtures of

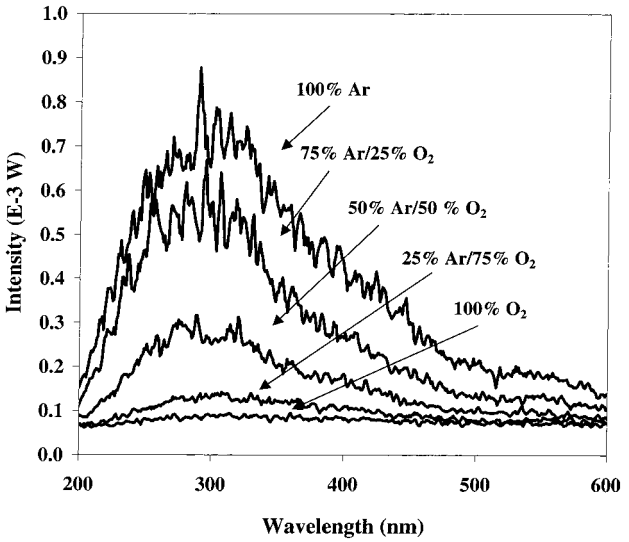

Figure 3. SL spectra at 358 kHz with saturation gases. Ar and O_2 are present at various ratios. Oxygen quenching of sonoluminescence is observed; as the percentage of O_2 increases, the luminescence intensity decreases over the entire spectrum.

Ar and O_2, as shown in Figure 3. The frequency used for these experiments was 358 kHz. The decrease in signal intensity follows the decrease in percentage of Ar. The features of each spectrum at different sparge ratios are analogous although the intensities differ. There was virtually no spectral emission observed in the presence of 100% O_2. Likewise, as shown in Figure 3, the spectra at various sparge gas ratios at 358 kHz vary primarily in total intensity and not in distinctive spectral features.

Numerous investigations of aqueous SL provide evidence of collisions between gas-phase molecules that, upon bubble collapse, create high-energy species capable of light emission.[13,23] The kinetic energy of water molecules within the bubble can be converted into internal energy via inelastic collisions (M is an inert third molecule such as argon):

$$H_2O + M \rightarrow H_2O^* + M \quad (1)$$

Upon collision, these molecules can be excited into various rotational, vibrational, and electronic states.[24] Excited water molecules will relax through a transition state (via reaction 2) producing a luminescence continuum in the region of 380−600 nm ($\lambda_{max} \sim 425$ nm).[24]

$$H_2O^* \rightarrow H_2O + h\nu_1 \quad (2)$$

At a sufficient energy, the water molecule may dissociate into a hydrogen atom and a hydroxyl radical in either the ground (reaction 3) or excited state (reaction 4):

$$H_2O \rightarrow H + {}^{\bullet}OH \quad (3)$$

The excited hydroxyl radical will emit at $\lambda \sim 280$, 310, and

$$H_2O \rightarrow H + {}^{\bullet}OH^* \rightarrow H + {}^{\bullet}OH + h\nu_2 \quad (4)$$

340 nm [1] and exhibits an emission continuum in the region $\lambda \sim 200-400$ nm.[25]

Hydroxyl radicals formed in the gas phase may recombine to form hydrogen peroxide or initiate reactions with other species within and near the bubble. Inelastic collisions may occur with hydroxyl radicals in the ground state subsequently producing excited species with emission maxima at 310 nm:[1,25]

$$^{\bullet}OH + M \rightarrow {}^{\bullet}OH^* + M \rightarrow {}^{\bullet}OH + M + h\nu_3 \quad (5)$$

Reactions 4 and 5 are considered predominant during acoustic cavitation and are consistent with the spectra in Figures 2 and 3 exhibiting peak maxima at approximately 310 nm. It is difficult to differentiate between peaks due solely to emission from the excited-state hydroxyl radical and peaks due to other species because of the broad continuum. Furthermore, the radiative recombination between H and $^{\bullet}$OH may contribute to SL:

$$H + {}^{\bullet}OH + M \rightarrow [H\cdots OH\cdots M]^{\#} \rightarrow H_2O + M + h\nu_4 \quad (6)$$

Here # denotes a vibrationally excited quasi-molecule which emits at $\lambda \sim 400$ nm.[25−27]

The formations of excimer molecules such as (M$^{\bullet}$OH)*, M_2*, and (M$^{\bullet}H_2O$)* are also possible because of the immense transient pressures and densities created upon bubble implosion; the excimer will contribute to the broad continuum at lower wavelengths. These excimers are formed by three-body collisions

$$H_2O^* + 2M \rightarrow H_2O^*{}^{\bullet}M + M \rightarrow H_2O{}^{\bullet}M + M + h\nu_5 \quad (7)$$

and emit at $\lambda < 300$ nm.[28] This process occurs at short distances between H_2O* and M, where the collisional potential is equal to or greater than thermal energy, because, in this situation, a third species may remove the excess kinetic energy of H_2O and M. In the presence of argon, the only inert species in our system, Ar$^{\bullet}$OH* ($\lambda \sim 310$, 316, and 318 nm) and Ar$^{\bullet}$HO* ($\lambda \sim 340$ nm) excimers, can exist:[29]

$$Ar + OH^* \rightarrow Ar{}^{\bullet}OH^* \ (Ar{}^{\bullet}HO^*) \rightarrow Ar + OH + h\nu_6 \quad (8)$$

The spectral features at different frequencies (Figure 2) indicate that the fundamental mechanisms of SL are similar during irradiation with any of the frequencies in this study. Since SL is known to originate from the gas phase and not from the interface or bulk solution, bubble implosion at 205, 358, and 618 kHz provides energetically favorable conditions for luminescent type reactions.[30] The lower intensity emission spectrum observed at 1071 kHz may be due to two factors: (1) Adiabatic bubble collapse at 1071 kHz provides the least amount of energy to initiate luminescence reactions. (2) The rapid expansion and collapse of bubbles during acoustic cavitation takes place at a rate that is able to sufficiently quench a significant number of energetic molecules before they luminesce.

Oxygen is known to be a significant quencher of chemiluminescence.[31] The SL spectra formed at 358 kHz in the presence of different sparge gas ratios of Ar and O_2 (Figure 3) suggests the importance of O_2 in SL emission quenching.

Aqueous Cavitation Chemistry. The rate constants for 1,4-dioxane decomposition were determined and compared to the luminescence intensity at 358 kHz and corresponding gas sparges. Normalized values for SL intensity and pseudo-first-order kinetic rate constants are shown in Figure 4. The values are normalized with respect to the maximum intensity or rate constant at each frequency. The SL intensity is greatest at 100% Ar and declines with decreasing Ar sparge ratio. The optimal decomposition rate for 1,4-dioxane is observed when a sparge ratio of 75% Ar/25% O_2 is employed, and the rate decreases with lower Ar ratios although not as significantly as the emission intensity. 1,4-Dioxane is postulated to decompose predominantly in the interfacial region and bulk solution through a series of free radical oxidation pathways.[20]

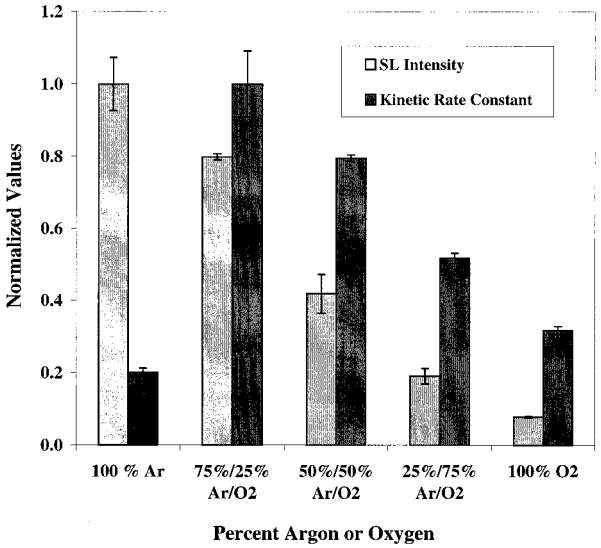

Figure 4. Relative SL intensities and 1,4-dioxane pseudo-first-order decomposition rate constants at various saturation gas ratios. All normalized SL intensities and decomposition rate constants are given as a fraction of the highest value of all gas ratios. Frequency = 358 kHz. Error bars represent one standard deviation.

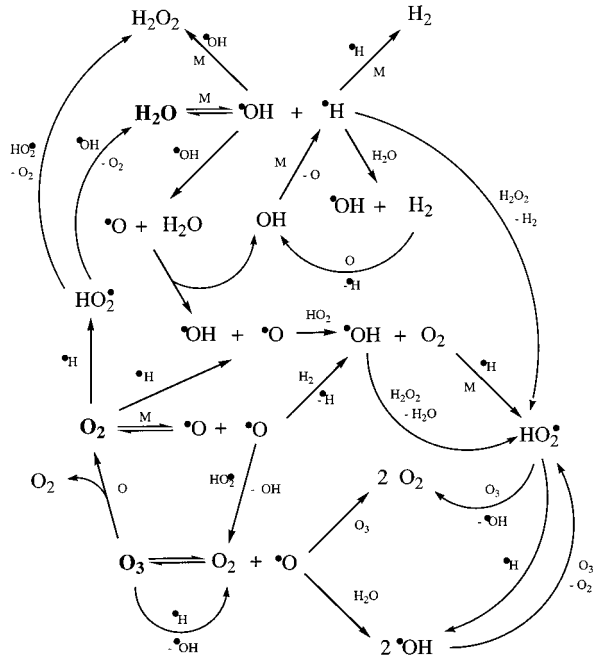

Figure 5. Chemical reactions during acoustic cavitation in the presence of oxygen, ozone, or an inert gas (M). M is an inert third molecule such as argon. The •OH radical is assumed to play the most significant role in sonochemical reactions although other free radicals ($HO^{\bullet}_2$, •O) may be important oxidizing species as well.

To understand these two data sets, it is necessary to consider the series of complex reactions that take place within the cavitation bubble during ultrasonic irradiation (see Figure 5).[32] The presence of an inert saturation gas such as argon during aqueous sonication will promote a number of principal reactions within the microbubble (M is an inert third molecule). The thermolysis of H_2O to form hydroxyl radical and hydrogen atom is one of the most prevalent reactions during sonication of aqueous solutions.[14] Hydroxyl radicals have been specifically identified in sonicated aqueous solutions via electron spin resonance.[33] The •OH radical is considered the primary oxidizing species during aqueous sonication. The resulting •OH radicals react with hydrogen to form water, react with another •OH radical to form hydrogen peroxide, or promote decomposition of an organic constituent.[21]

Ultrasonic irradiation in the presence of oxygen will engender additional reactions within the gaseous bubble phase (Figure 5).[32,34,35] Sonolytic reactions of O_2 lead to •OH, •OOH, and •O radicals that provide other reactive species. The production of oxygen atoms (•O)[34,35] and hydroperoxyl radicals (•OOH)[34,36] has been inferred from the involvement of these species in specific sonochemical reactions. The •O atom, due to its highly reactive nature in the gaseous phase,[32] is more likely to play an indirect role by providing radical species (through reaction with oxygen and water vapor) with longer lifetimes that can subsequently move to the interfacial region and react with a target compound.[37,38] H_2O_2 results primarily from the recombination of •OH radicals.[21,39] All free radicals may react with other molecules encountered within and around the cavitation bubble.

SL and cavitation chemistry will be influenced by the type of saturation gas used. The temperature in the center of a collapsed cavitation bubble can be estimated with the following equation:

$$T_{max} = T_0\left\{\frac{P_m(K-1)}{P}\right\} = T_0\left(\frac{R_0}{R_{min}}\right)^{3(K-1)} \qquad (9)$$

where T_0 = temperature of the bulk solution, K = polytropic index of the saturation gas ($K \simeq C_p/C_v$), P = pressure in the bubble at its maximum size, P_m = pressure in the bubble upon collapse, R = resonance bubble radius, and R_{min} = bubble radius upon collapse.[40,41] During acoustic cavitation, gases with high polytropic indices and low thermal conductivities will lead to more intense conditions within a collapsing bubble because less heat is dissipated to the surrounding aqueous environment during the rapid implosion.[10,34] The polytropic index, K, correlates to the heat released upon gas compression and is higher for Ar than for O_2 (1.66 vs 1.41),[42] and the thermal conductivity of O_2 is higher than that of Ar (48.1 vs 30.6 mW/(m K)).[43] Therefore, the bubble implosion in the presence of Ar favors a higher overall temperature. The production of additional radical species during decomposition of O_2 as shown in Figure 5, however, can compensate for the lower internal cavitation temperatures. Nevertheless, a combination of the sparge gases O_2 and Ar leads to faster degradation rates than either gas individually; the fastest degradation rate occurs at a 75% Ar/25% O_2 ratio which creates an optimum balance between the higher temperatures generated during acoustic cavitation from Ar and the generation of additional active radical species from O_2. This approximate ratio has also been demonstrated to be optimal by other investigators.[34]

The greatest SL intensity and the slowest 1,4-dioxane decomposition rate occur in the presence of a 100% Ar sparge during sonication at 358 kHz. This difference reflects the higher temperatures formed upon bubble collapse in the presence of Ar. Higher temperatures favor reactions that produce emitting species.[44] In addition, a greater variety of luminescence reactions proceed in the absence of O_2. In the absence of O_2, however, fewer oxidizing free radical species are released into the solution, so that 1,4-dioxane decomposition is slowest in this case.

Frequency Effects. To further understand the role of frequency during ultrasonic irradiation, the kinetics of H_2O_2 generation and 1,4-dioxane decomposition[20] were measured at corresponding ultrasonic frequencies (gas sparge ratio 75% Ar/25% O_2). H_2O_2 exhibits zero-order kinetics and results from the recombination of •OH radicals. Normalized values for kinetic

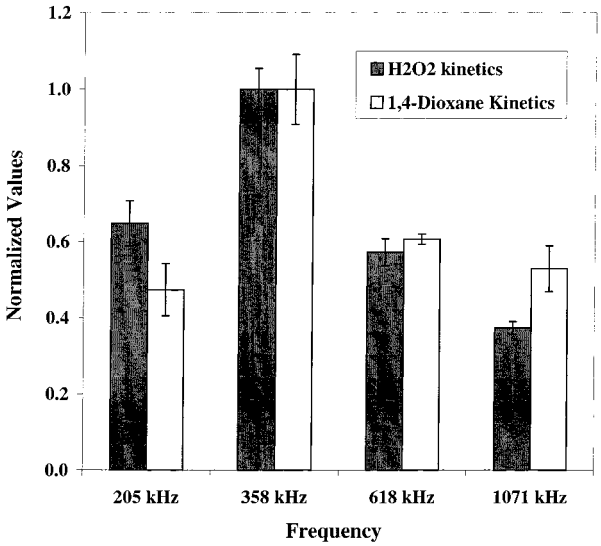

Figure 6. Normalized H_2O_2 kinetic constants and 1,4-dioxane decomposition rate constants at four frequencies (205, 358, 618, and 1071 kHz). The ratio of saturation gas used is 75% Ar/25% O_2. Reactor temperature was 25 °C. Error bars represent one standard deviation.

rates are shown in Figure 6 and are highest at 358 kHz. The slowest H_2O_2 formation rate is observed at 1071 kHz whereas the slowest 1,4-dioxane decomposition rate takes place at 205 kHz.

Previous investigations have shown that frequency plays an important role in sonolytic processes.[9,45] There is a limited understanding, however, of the fundamental mechanisms behind frequency effects. To discuss the frequency effects in greater detail, additional aspects of bubble behavior must be considered. Microcavities may undergo the following: (1) periodic size oscillations (stable cavitation); (2) disintegration or fragmentation; (3) rapid expansion and collapse (transient or acoustic cavitation); (4) escape from solution due to mass convection and buoyancy.[25,32] Chemical reactivity and SL are strictly a result of stable and transient cavitation processes, but the others (2 and 4) may influence the degree of cavitation activity. The relative probably of each process depends on the bubble size, applied power, and frequency. An outline of the most significant fundamental mechanisms of ultrasonic irradiation related to frequency is shown in Figure 7.

After a number of radial oscillations generated by ultrasonic waves, a microbubble will reach a resonance size immediately before implosion. The resonance size of the acoustic bubble is inversely correlated to the emitted frequency.[46] It is given by the following equation:

$$R_r^2 = \frac{3KP_0}{\rho\omega_r^2} \tag{10}$$

Here R_r is the resonant bubble radius, κ ($\kappa = C_p/C_v$) is the polytropic index, P_0 is the hydrostatic pressure, ρ is the density of the solution, and ω_r is the resonant frequency. Although a range of bubble radii will exist at any particular frequency, bubbles with the resonance size given by eq 10 will constitute the majority of effective cavitation events.[46] As frequency increases, the resonant radius of acoustic bubbles decreases and, correspondingly, collapse times decrease as well. The bubble collapse time, τ, for a gas or vapor filled void in an incompressible liquid is

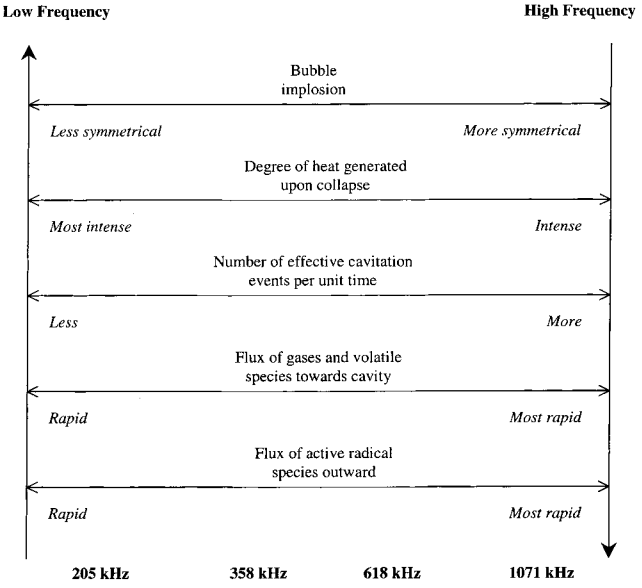

Figure 7. Scheme of acoustic cavitation events as a function of frequency during continuous ultrasonic irradiation and gas sparging. Vertical arrows designate increasing order of importance with respect to sonochemical activity as a function of frequency. At lower frequencies, it is hypothesized that a significant fraction of cavitation bubbles will collapse asymmetrically while greater gas and volatile species flux rates occur at higher ultrasonic frequencies.

$$\tau = 0.915R_m\left\{\frac{\rho}{P_m}\right\}^{1/2}\left(1 + \frac{P_{vg}}{P_m}\right) \tag{11}$$

where R_m = bubble radius at the beginning of collapse, ρ = density of the liquid, P_m = pressure in the liquid, and P_{vg} = pressure in the bubble at the start of bubble collapse.[47] The resonant radius, bubble surface area, and bubble collapse time as a function of ultrasonic frequency are compared in Table 2. Assuming an adiabatic collapse and the presence of the same sparge gas, lower frequencies will lead to a more violent collapse than higher frequencies due to greater resonant bubble sizes.[7] Evidence for this has been corroborated by studies on SL[27] and acoustic cavitation field predictions combining mathematical modeling with ultrasonic experimental observations.[48]

At higher frequencies, smaller bubbles require fewer acoustic cycles before reaching the requisite resonant size. This leads to transient cavitation events occurring at a faster rate per unit time as the frequency is increased because bubble lifetimes are shorter. A greater number of oscillations increase the mass transfer of •OH radicals into the surrounding medium and concurrently increase diffusion of gases and volatile compounds into the bubble.[45] At high frequencies, however, the resonance bubble size may not be large enough to produce enough energy upon collapse to form sufficient numbers of •OH radicals from water, and a point of diminishing returns is reached. From Figure 6, it is observed that the frequency range proximal to 358 kHz appears to optimize both energy from bubble implosion and a concomitant mass transfer of reactive species into and out of the bubble. This is true for 1,4-dioxane degradation and H_2O_2 generation. As the frequency increases, the intensity of bubble implosions lessens, but the faster flux of active radical species and bulk chemical compounds toward the cavitation bubble interface induced at 1071 kHz may explain why the 1,4-dioxane decomposition rate is still significant at this frequency.

Apart from sound waves, there are a number of other forces acting upon a bubble during acoustic cavitation. They include buoyancy, radiative pressures, and Bjerkness forces induced by

TABLE 2: Influence of Frequency on Microbubble Characteristics during Acoustic Cavitation[a]

freq (kHz)	reson radius (μm)	surf area A (μm^2)	vol (V) (nL)	A/V (μm^{-1})	collapse time (μs)
205	17.5	3.85×10^3	2.24×10^{-2}	0.17	1.59
358	10.0	1.26×10^3	4.19×10^{-3}	0.30	0.91
618	5.8	4.23×10^2	8.17×10^{-4}	0.52	0.53
1071	3.3	1.37×10^2	1.51×10^{-4}	0.91	0.30

[a] Dissolved gas: argon. These are theoretical values calculated according to eqs 10 and 11; the bubble radii were not measured in this study.

TABLE 3: Effect of Bicarbonate on Sonoluminescence Intensity and H_2O_2 Formation via Recombination of $^{\bullet}$OH Radicals Produced during Aqueous Ultrasonic Irradiation[a]

	frequency (kHz)			
	205	358	618	1071
SL intensity (% decrease)	21.5	30.0	20.0	1.4
H_2O_2 production (% decrease)	67.4	68.6	70.8	85.4

[a] Bicarbonate = 50 MM HCO_3^-. The concentration of bicarbonate was the same for all studies at each frequency. Numbers represent % reduction of either the SL signal or H_2O_2 kinetic rate caused by bicarbonate addition.

other oscillating bubbles.[49] These processes are known to induce an asymmetrical collapse or fragmention during cavity implosion. If the acoustic field and surrounding external forces are adequately intense, surface distortions can arise from interfacial instability (more likely near solid surfaces) resulting in microjets or microstreams leading to fragmentation. The extent of fragmentation is related to the size of the bubble, and at lower frequencies, a significant fraction of bubbles will collapse in this way.[50]

Bubble fragmentation, or incomplete symmetric bubble collapse, will have more important implications for chemical reactivity at lower frequencies (Figure 7). Even during asymmetrical bubble implosions, high temperatures and pressures may be reached because a high-speed adiabatic collapse still takes place. At lower frequencies, where bubble distortions are more likely, microjetting through the microcavity interface will bring bulk solution species to the reactive center. In this situation, a greater percentage of nonvolatile species is exposed to the extreme conditions associated with SL.

To further corroborate the explanation for frequency effects, SL intensity was compared in the presence and absence of bicarbonate, a $^{\bullet}$OH radical scavenger. The influence of bicarbonate (50 mM HCO_3^-) as a percent reduction in SL is seen in Table 3. These results indicate that bicarbonate reduces SL intensity at 205, 358, and 618 kHz. Bicarbonate, however, has little effect at 1071 kHz. Since SL reactions only take place within the microcavity,[27,30] bicarbonate should not impact luminescence at all. This is the case at 1071 kHz; the change in SL is negligible. However, at lower frequencies (205, 358, and 618 kHz), a significant reduction occurs. This can be attributed to microjetting and streaming caused by cavity disruption that is more likely to occur at lower frequencies and larger resonant bubble radii. Several studies of the sonoluminescence of alkali metal salts[51] and metal carbonyls[2] show luminescent emission exhibited from metal species within the gas phase region of the microbubble. Thus, bubble dynamics leading metal ionic species to emit within a cavitation bubble will likely allow for bicarbonate species to be present there as well.

The rates for H_2O_2 production were also determined in the presence of bicarbonate. The experiments indicate that bicarbonate inhibits H_2O_2 production as well; the percentage decreases from the original production rates are listed in Table 3. The largest diminution in H_2O_2 generation takes place at 1071 kHz and decreases in order of descending frequency. The production of H_2O_2 reflects the hydroxyl radical production in cavitation bubbles. Since bicarbonate is an ion, it will scavenge free radicals predominantly in the bulk water phase or near the bubble interface. From previous investigations, H_2O_2 has been estimated to form predominantly in the interfacial region where a very high local $^{\bullet}$OH radical population exists.[21] If this is the case, then the frequency that allows the greatest flux of $^{\bullet}$OH radicals to the interface region, where scavenging bicarbonate ions can easily access, would be impacted the most. From Table 3, the greatest reduction in H_2O_2 production due to bicarbonate addition occurs at 1071 kHz (highest flux rate). The impact of bicarbonate is less significant as frequency and commensurate radical flux rates decrease.

Conclusion

Describing acoustic cavitation conditions at different frequencies during ultrasonic irradiation is an arduous task. Important processes and variables that must be considered include mass transfer through the gas−liquid interface, effective cavitation events per unit time, resonant bubble size, deformation of the interface during bubble collapse, and temperatures within the microcavity. This investigation contributes to explanations of the broad spectra produced at different frequencies. Oxygen appears to be a significant quencher of these luminescence reactions. A descriptive scheme of the mechanisms at discrete ultrasonic frequencies promoting SL and sonochemical reactivity is also presented. Nonlinear bubble implosions play a more significant role at lower frequencies whereas higher species flux rates influence chemical reactivity at higher frequencies. Finally, the optimal frequency for SL and chemical reaction rates is 358 kHz.

Acknowledgment. The authors wish to thank the United States Department of Energy (DOE Grant No. DE-FG07-96ER14710) and The Purdue Research Foundation (Award No. 6902949) for funding these studies. The authors also thank Dr. Changhe Xiao of the School of Civil Engineering at Purdue University for analytical laboratory assistance.

References and Notes

(1) Didenko, Y. T.; McNamara, W. B., III; Suslick, K. S. *J. Phys. Chem. A* **1999**, *103*, 10783−10788.
(2) Suslick, K. S.; Flint, E. B.; Grinstaff, M. W.; Kemper, K. A. *J. Phys. Chem.* **1993**, *97*, 3098−3099.
(3) Hoffmann, M. R.; Hua, I.; Hochemer, R. *Ultrason. Sonochem.* **1996**, *3*, S163−S172.
(4) Flint, E. B.; Suslick, K. S. *Science* **1991**, *253*, 1397−1399.
(5) Suslick, K. S.; Kemper, K. A.; Flint, E. B. *Proc. IEEE Ultrason. Symp.* **1993**, *2*, 777−783.
(6) Portlanger, G.; Heusinger, H. *Ultrason. Sonochem.* **1997**, *4*, 127−130.
(7) Petrier, C.; Jeunet, A.; Luche, J.-L.; Reverdy, G. *J. Am. Chem. Soc.* **1992**, *114*, 3148−3150.
(8) Entezari, M. H.; Kruus, P. *Ultrason. Sonchem.* **1994**, *1*, S75−S77.
(9) Cum, G.; Galli, G.; Gallo, R.; Spadaro, A. *Ultrasonics* **1992**, *30*, 267−270.
(10) Hua, I.; Hoffman, M. *Environ. Sci. Technol.* **1997**, *31*, 2237−2243.
(11) Hiller, R.; Weninger, K.; Putterman, S. J.; Barber, B. P. *Science* **1994**, *266*, 248−250.
(12) Birot, A.; Brunet, H.; Galy, J.; Millet, P. *J. Chem. Phys.* **1975**, *63*, 1469−1473.
(13) Didenko, Y. T.; Gordeychuk, T. V.; Koretz, V. L. *J. Sound Vib.* **1991**, *147*, 409−416.
(14) Suslick, K. S. *Ultrasound: Its Chemical, Physical and Biological Effects*; VCH Publishers: New York, 1988.

(15) Kimura, T.; Sakamoto, T.; Leveque, J.; Sohmiya, H.; Fujita, M.; Ikeda, S.; Ando, T. *Ultrason. Sonochem.* **1996**, *3*, S157−161.
(16) Finch, R. D. *Br. J. Appl. Phys.* **1965**, *16*, 1543−1553.
(17) Sehgal, C.; Sutherland, R. G.; Verrall, R. E. *J. Phys. Chem.* **1980**, *84*, 525−528.
(18) Didenko, Y. T.; Nastich, D. N.; Pugach, S. P.; Polovinka, Y. A.; Kvochka, V. I. *Ultrasonics* **1994**, *32*, 71−76.
(19) Entezari, M. H.; Kruus, P. *Ultrason. Sonochem.* **1994**, *2*, 19−24.
(20) Beckett, M. A.; Hua, I. *Environ. Sci. Technol.* **2000**, *34*, 3944−3953.
(21) Henglein, A.; Kormann, C. *Int. J. Radiat. Biol.* **1985**, *48*, 251−258.
(22) Kormann, C.; Bahnemann, D. W.; Hoffmann, M. R. *Environ. Sci. Technol.* **1988**, *22*, 798−806.
(23) Didenko, Y. T.; Pugach, S. P. *Ultrason. Sonochem.* **1994**, *1*, S9−S12.
(24) Engel, V.; Meijer, G.; Bath, A.; Andresen, P.; Schinke, R. *J. Chem. Phys.* **1987**, *87*, 4310−4314.
(25) Sehgal, C.; Sutherland, R. G.; Verrall, R. E. *J. Phys. Chem.* **1980**, *84*, 388−395.
(26) Saksena, T. K.; Nyborg, W. L. *J. Phys. Chem.* **1970**, *53*, 1722−1734.
(27) Walton, A. J.; Reynolds, G. T. *Adv. Phys.* **1984**, *33*, 595−660.
(28) Didenko, Y. T.; Pugach, S. P. *J. Phys. Chem.* **1994**, *98*, 9742−9749.
(29) Lemaire, J. L.; Tchang-Brillet, W. U. L.; Shafizadeh, N.; Rostas, F.; Rostas, J. *J. Phys. Chem.* **1989**, *91*, 6657−6663.
(30) Ashokkumar, M.; Hall, R.; Mulvaney, P.; Grieser, R. *J. Phys. Chem. B* **1997**, *101*, 10845−10850.
(31) Carraway, E. R.; Demas, J. N. *Langmuir* **1991**, *7*, 2991−2998.
(32) Colussi, A. J.; Weavers, L. K.; Hoffmann, M. R. *J. Phys. Chem. A* **1998**, *102*, 6927−6934.
(33) Makino, K.; Mossoba, M. M.; Riesz, P. *J. Phys. Chem.* **1983**, *87*, 1369−1377.
(34) Hart, E. J.; Henglein, A. *J. Phys. Chem.* **1985**, *89*, 4342−4347.
(35) Fischer, C. H.; Hart, E. J.; Henglein, A. *J. Phys. Chem.* **1986**, *90*, 1954−1956.
(36) Suslick, K. S.; Grinstaff, M. W. *J. Am. Chem. Soc.* **1990**, *112*, 7807.
(37) Fang, X.; Mark, G.; Von Sonntag, C. *Ultrason. Sonochem.* **1996**, *3*, 57−63.
(38) Hart, E. J.; Fischer, C.-H.; Henglein, A. *J. Phys. Chem.* **1986**, *90*, 5989−5991.
(39) Anbar, M.; Pecht, I. *J. Phys. Chem.* **1964**, *68*, 352−355.
(40) Noltingk, B. E.; Nepprias, E. A. *Proc. Phys. Soc. B* **1950**, *63B*, 674.
(41) Neppiras, E. A.; Noltingk, B. E. *Proc. Phys. Soc. B* **1951**, *63B*, 1032.
(42) *CRC Handbook of Chemistry and Physics*, 77th ed.; CRC Press: Boca Raton, FL, 1996.
(43) Kang, J. W.; Hung, H. M.; Lin, A.; Hoffmann, M. R. *Environ. Sci. Technol.* **1999**, *33*, 3199−3205.
(44) Ashokkumar, M.; Grieser, F. *Ultrason. Sonochem.* **1999**, *6*, 1−5.
(45) Hung, H.-M.; Hoffmann, M. R. *J. Phys. Chem. A* **1999**, *103*, 2734−2739.
(46) Leighton, T. G. *The Acoustic Bubble*; Harcourt Brace & Co.: Orlando, FL, 1994.
(47) Mason, T. J.; Lorimer, J. P. *Ultrasound: Theory, Applications and Uses of Ultrasound Chemistry*; Ellis Horwood Limited: Chichester, U.K., 1991.
(48) Laborde, J. L.; Bouyer, C.; Caltagirone, J. P.; Gerard, A. *Ultrasonics* **1998**, *36*, 581−587.
(49) Lepoint, T.; Mullie, F. *Ultrason. Sonochem.* **1994**, *1*, S13−S21.
(50) Matula, T. J.; Roy, R. A.; Mourad, P. D.; McNamara, W. B., III; Suslick, K. S. *Phys. Rev. Lett.* **1995**, *75*, 2602−2605.
(51) Sehgal, C.; Steer, R. P.; Sutherland, R. G.; Verrall, R. E. *J. Phys. Chem.* **1979**, *70*, 2242−2248.